www.czasopisma.pan.pl PAN www.journals.pan.pl

ARCHIVES of FOUNDRY ENGINEERING

DE GRUYTER OPEN

DOI: 10.1515/afe-2017-0133

ISSN (2299-2944)
Volume 17
Issue 4/2017

Published quarterly as the organ of the Foundry Commission of the Polish Academy of Sciences

73 – 78

Microstructural and Mechanical Characterization of Al-0.80Mg-0.85Si-0.3Zr Alloy

F. Kahrıman *, M. Zeren
Kocaeli University, Metallurgical and Materials Engineering Department,
Umuttepe Campus, 41380 Kocaeli Turkey
*Corresponding author. E-mail address: fulya.kahriman@kocaeli.edu.tr

Received 28.04.2017; accepted in revised form 05.07.2017

Abstract

In this study, Al-0.80Mg-0.85Si alloy was modified with the addition of 0.3 wt.-% zirconium and the variation of microstructural features and mechanical properties were investigated. In order to produce the billets, vertical direct chill casting method was used and billets were homogenized at 580 °C for 6 h. Homogenized billets were subjected to aging practice following three stages: (i) solution annealing at 550 °C for 3 h, (ii) quenching in water, (iii) aging at 180 °C between 0 and 20 h. The hardness measurements were performed for the alloys following the aging process. It was observed that peak hardness value of Al-0.80Mg-0.85Si alloy increased with the addition of zirconium. This finding was very useful to obtain aging parameters for the extruded hollow profiles which are commonly used in automotive industry. Standard tensile tests were applied to aged profiles at room temperature and the results showed that modified alloy had higher mechanical properties compared to the non-modified alloy.

Keywords: Solidification process, Heat treatment, Metallography, Microstructure, Mechanical properties

1. Introduction

Aluminium alloys are the focus of many researchers as structural materials that can be developed for many applications. Especially automotive industry and construction industries desire to produce lightweight parts with good plasticity, excellent corrosion resistance and good weldability and lower scrap rates. The heat treatable Al-Mg-Si alloys are often preferred for these applications. Alloying elements affect not only the microstructural features but also physical and mechanical properties. Among these alloying elements, Mn is used to control the grain structure resulting in the enhancement of strength [1-6]. The wear performance of these alloys can be improved by adding of Si and Cu also has positive effect on the corrosion resistance. New trends on the enhancement of mechanical properties rely on the addition of Zr, Hf, Sc and V. Several reports revealed that these elements provided a combination of grain refinement and precipitation hardening effects to improve the properties [2-5]. The addition of Zr leads to form Al_3Zr precipitates during solidification [7-8]. These precipitates impede grain boundary mobility together with free dislocations and thereby restrict grain growth. Thus, these effects enhance the thermal stability when the alloy is exposed to higher temperatures during thermo-mechanical processes such as extrusion [9-11].

In this study, the effect of Zr on microstructural features and mechanical properties of Al-0.80Mg-0.85Si alloy were investigated. The modified alloy is heat treatable and the mechanical properties of the alloy were investigated as a function of artificial aging heat treatment.

2. Experimental study

The alloys used in the experimental study were cast industrially with vertical billet caster in the form of 2000 mm long, 152 mm diameter billets. These billets were homogenized at 580 °C for 6 h and subsequently cooled to room temperature. The chemical compositions of the alloys are presented in Table 1. Chemical composition of the first alloy corresponds to the Al-0.80Mg-0.85Si alloy. The second alloy has a similar composition as the first one but also contains 0.3 % wt. zirconium. Zr was added in the form of a master Al-10%Zr alloy. Oxford instruments foundry-master UV optical emission spectrometer was used for elemental analysis of the alloys. The analyses were repeated three times and the mean values were reported for each element.

Table 1.
The chemical compositions of the alloys used in the present study (wt.-%).

Alloys	Al	Si	Fe	Cu	Mn	Mg	Ti	Zr
A	Bal.	0.87	0.27	0.01	0.64	0.83	0.01	0.02
B	Bal.	0.82	0.25	0.02	0.50	0.80	0.01	0.32

Metallographic samples were prepared according to the standard preparation procedure grinding with SiC paper (320, 600, 1000 and 2500 grit size) and polishing with 3 and 1 µm diamond suspensions, respectively. Chemical etching was performed by Keller's reagent. The microstructures of the alloys were examined using Nikon Eclipse L150A light microscope (LM) and Jeol JSM-6060 scanning electron microscope (SEM). The average grain sizes (equivalent circle diameter) in the microstructure of the alloys were detected using NIS Elements Basic Research Software. IXRF model energy dispersive spectrometer (EDX) attached SEM was used for microanalysis. X-ray diffraction (XRD) analyses were done using a Rigaku SA-HF3 X-ray diffractometer with CuKα (λ =1.54 Å) radiation (40 kV and 20 mA) to determine the intermetallic compounds. The obtained diffraction patterns were collected from 10° to 90° at a scanning rate of 1.0°/min. The macro-hardness (HV1) of the alloys was measured using Vickers hardness tester (digital FV-700, Future-Tech) with 1 kgf load. The averages of at least five separate measurements per sample, taken randomly on the surface, were reported. Tensile specimens were prepared according to the DIN EN 10002-1 standard and tensile tests were performed by Zwick / Roell Z250 tensile testing machine at room temperature.

3. Results and discussion

3.1. Microstructural characterization

Figure 1 a and b present the microstructures of the investigated alloys in as-cast condition. Figure 1a shows that a typical as-cast microstructure of Alloy A. The microstructure consists of coarse grains including the α-Al dendrites and several precipitates in the interdendritic regions. In the as-cast state, well-known precipitates such as rod-like shaped eutectic Mg_2Si, skeleton shaped α-AlFeMnSi and β-AlFeSi exist in the interdendritic regions [12-13]. The average grain size for the Alloy A was 496,67 µm ± 180 in diameter and 432,52 µm ± 167 in diameter for Alloy B in as-cast state. The addition of Zr was not having significant effect on refinement of the average grain size, but there was a great effect on refinement of the dendritic structure. In Figure 1b it can be observed that dendritic structure of the Alloy B is refined compared to Alloy A by Zr addition. Besides, it has a homogeneous equiaxed dendritic structure and more uniform distribution of the second phases in the interdendritic regions. This is in agreement with some of the literature concluding that even minor Zr addition has considerable effect on the microstructure refinement of aluminium alloys due to presence of Zr-bearing precipitates [2-10]. Microstructures of the alloys after homogenization are shown in Figure 1 c and d. After the homogenization of the alloys at 580 °C, interconnected plate-like β-AlFeSi intermetallics may transform to more spheroidal discrete α-AlFeMnSi phase. This transformation is important since it enhances ductility of the alloy. Mg_2Si phase precipitates as dispersed particles [13].

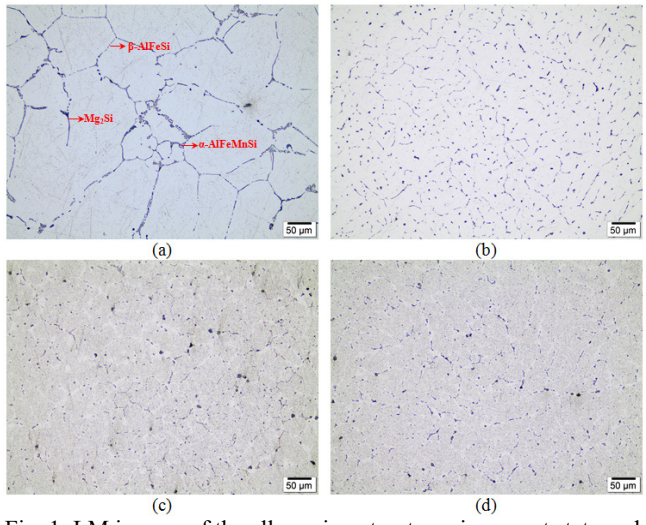

Fig. 1. LM images of the alloy microstructures in as-cast state and homogenized at 580 °C for 6h a, c) Alloy A, b, d) Alloy B

XRD spectra of the alloys in as-cast and homogenized conditions are shown in Figure 2. The spectrum of Alloy B in homogenized condition presents the strongest peaks among the others; clearly indicating the increase in the volume fraction of precipitates. Furthermore, Zr-bearing precipitates were also determined by EDX spot analysis during SEM examinations. In Figure 3, EDX spot analysis of the rod-shaped phase revealed the presence of small amount of Si, apart from Al, and Zr. Zirconium forms fine and metastable Al_3Zr precipitates in the $L1_2$ structure, coherent with the Al matrix, forming during the decomposition of supersaturated solid solution. Their pinning effect can have a huge impact of improving the microstructural properties of aluminium alloys. These precipitates can transform to the equilibrium $D0_{23}$-Al_3Zr structure during prolonged heat treatment. In 6xxx

aluminium alloys with high content of Si, the $(Al,Si)_3Zr$ precipitate which has $D0_{22}$ structure is formed in place of the equilibrium $D0_{23}$ structure through substitution of Al by Si [7]. Crystal structure and lattice constants of Zr bearing precipitates are extremely similar to those of α-Al matrix, therefore they promote the heterogeneous nucleation during the solidification process of aluminium alloys and refine the grains of the alloys [9].

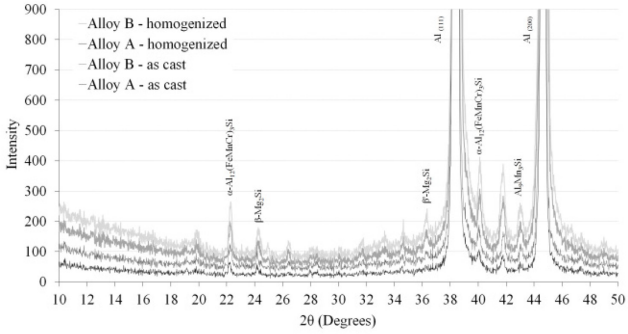

Fig. 2. X-ray diffraction spectra of the alloys in as-cast and homogenized conditions

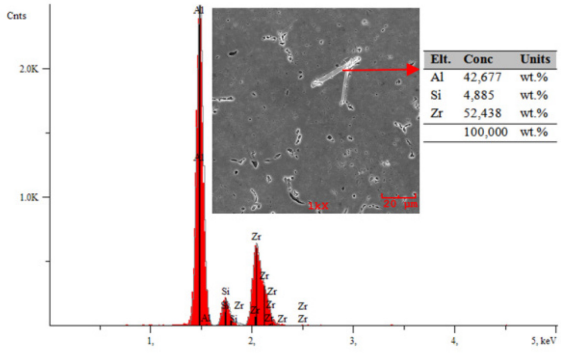

Fig. 3. SEM/EDX analysis of the Alloy B homogenized at 580 °C for 6h

3.2. Hardness measurements

Alloy B containing Zr (56.4 HV1) has much higher hardness than Alloy A (48.1 HV1) in as-cast state. The higher hardness is a result of more dispersed precipitates present in the microstructure. In addition, the hardness of the homogenized Alloy B (39 HV1) is higher than the homogenized Alloy A (36.7 HV1). It can be referred to the dissolution of hard phases and ensuing grain coarsening during holding at 580 °C for 6h. A large fraction of the alloying elements segregate and accumulate in the liquid phase during the casting of aluminum alloys and result in inhomogeneous alloying elements distribution in the microstructure. Therefore, removal of the inhomogeneous distribution of alloying elements on a microscale is achieved by homogenization treatment. The presence of eutectic constitutive particles with low melting points formed during solidification can also lead to segregation when they are located in the grain boundary or within the grains. Homogenization treatment of the alloys ensures dissolving these phases. In addition, there is, as expected, formation of some hard phases with sharp edges during casting. For example, Fe is the most common impurity in combination with certain alloying elements such as Mn and Si. These phases also negatively affect the hot workability and therefore the applicable ranges of process parameters during extrusion. These particles should be spheroidized by homogenization treatment [14].

3.3. Age hardening

An artificial aging cycle was applied to in order to investigate the effect of 0.3 % Zr addition on the precipitation hardening of the homogenized alloys. Commercial solution and aging heat-treating temperatures were applied to alloys in the experimental study since Alloy A is commonly used especially in the automotive industry. Therefore, aging time was the only process variable. Homogenized billets were subjected to a heat treatment sequence, consisting of (i) solution annealing at 550 °C for 3 h, (ii) quenching in water and (iii) artificial aging at 180 °C for 0-20 h. Figure 4 shows the hardness evolution of the alloys with aging time from which peak hardness values of the alloys could be determined. The peak hardness values for the alloys were achieved as 72.50 HV1 for Alloy A after 12 h of aging at 180 °C and as 80.90 HV1 for Alloy B after 16 h of aging at the same temperature. Thus, the addition of Zr resulted in an increased peak hardness at longer aging time. Furthermore, gradual decrease in hardness was much less in the Alloy B during over aging. In the aging of the ternary Al-Mg-Si alloys, previous studies showed that the precipitation sequence can be described as follows: supersaturated solid solution (α, SSS)→the coherent Guinier-Preston (GP) zones→needle shaped precipitates aligned along <100> directions of the matrix, which were coherent with the matrix (β'' phase)→rod-shaped precipitates, which were semi-coherent with the matrix (β' phase)→plate-shaped incoherent equilibrium precipitates (β phase of Mg_2Si composition). The hardness of the alloys reaches its peak value, when the density of needle-shaped β″ precipitates is maximum. In the experimental study, higher maximum hardness as a result of the addition of Zr to Alloy B was obtained at longer aging time due to the formation of Al_3Zr precipitates, which are coherent with the Al matrix and have $L1_2$ lattice structure. With further aging, hardness begins to decrease with the formation of the β′ and β precipitates. In the experimental study, the Al_3Zr precipitates which were coherent with the matrix and have $L1_2$ structure were transformed to the equilibrium Al_3Zr precipitate which were semi-coherent with the matrix and have $D0_{23}$ structure by prolonged aging heat treatment. However, the hardness was still higher compared to Alloy A without Zr. Alloys used in this investigation contain 0.80 Mg and 0.85 Si in weight percentage. Therefore, the increase in hardness of the alloys after aging at 180 °C for 12 or 16 h could be due to the precipitation of Mg_2Si phase particles. The strengthening of the alloys could also be explained by the interference of dislocation motion on account of the presence of precipitate particles of any other phase [15-18]. The dislocation-precipitate interaction in Al-Mg-Si alloys can be in two ways. When dislocations interact with a soft coherent precipitates, they can cut through around of the precipitates. If dislocations interact with hard incoherent precipitates, they can bypass them. These

dislocation-precipitate interactions give rise to strengthening of the alloy. Stacking fault energy, interfacial energy, coherency strain and lattice friction stress cause precipitation hardening due to coherent precipitates in Al-Mg-Si alloys. Coherent precipitates can lead to coherency strains due to the lattice mismatch between precipitate and matrix. Strain fields around the precipitate cause high local strength. Local strength increases with increasing precipitate radius, mismatch strains at interfaces and volume fraction of coherent precipitate. Local strength is reduced by displacement of the dislocation vector. The addition of Zr has a positive effect since the metastable Al_3Zr precipitates formed during the decomposition of the supersaturated solid solution. The coarsening rate of Zr-bearing precipitates is slower than that of without Zr. The thermal stability of Al_3Zr precipitates is directly influenced by the diffusivity of Zr within aluminum. At 400 °C, the diffusion coefficient of zirconium ($1.20x10^{-20}$ m^2/s) within aluminum is smaller than that of Cu ($2.27x10^{-14}$ m^2/s) or Mg ($6.14x10^{-14}$ m^2/s) [19]. Thus, Al_3Zr precipitates are thermally more stable than the conventional precipitates which provide precipitation hardening such as θ′-Al_2Cu or β′-Mg_2Si. All this information reveals why the phase transformation kinetic is slower in Zr-containing alloys [19-22].

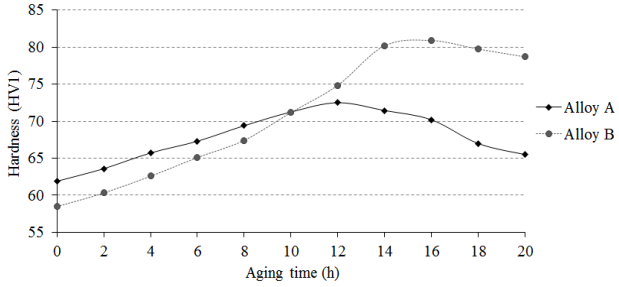

Fig. 4. Hardness evolution with aging time

The authors had investigated the effects of zirconium on phase transformation kinetic of the alloys in their previous work. They experimentally found Avrami equations using electrical conductivity and volume fraction of the precipitates within the Al-matrix. Electrical onductivity and volume fraction of precipitates have a linear relationship. The obtained phase transformation curves showed that the addition of zirconium to alloy slowed down the phase transformation kinetics. This finding is an approach to explain the recrystallization retarding behaviour of zirconium on aluminium alloy [23].

3.4. Tensile Properties and Fractography

Prior the tensile tests, extruded alloys were subjected to artificial aging process at optimum aging time after solution annealing at 560 °C for 3 h, subsequently quenching in water. Uniaxial tensile tests were performed on extruded hollow profiles at room temperature with deformation speed 20 mm/min. Four specimens taken parallel to the extrusion direction were tested for each alloy. The results of the tensile test are illustrated in Figure 5.

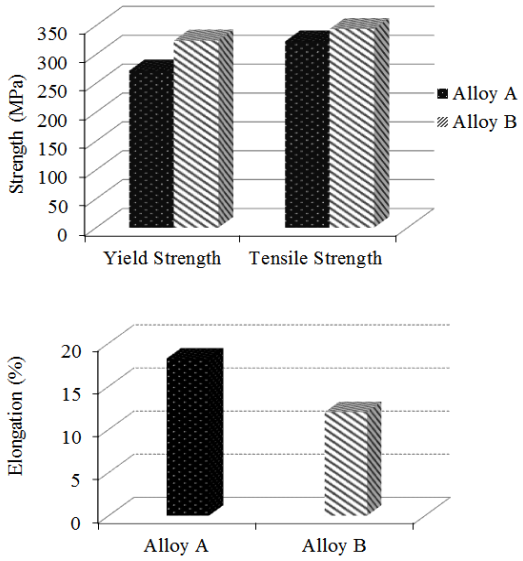

Fig. 5. Mechanical properties of the extruded alloys

It can be seen that the addition of Zr improved the yield strength of the extruded alloys from 272 MPa to 324 MPa. Besides, the ultimate tensile strength of the alloys increased from 322 MPa to 344 MPa, while the elongation decreases from 18% to 12%. Figure 6 shows the macro images of the fractured surfaces of the tensile specimens. When a sample is loaded by uniaxial tensile stress, direction of maximum shear stress is at 45º to the loading axis. Therefore, macro images of the tensile specimens support this argument.

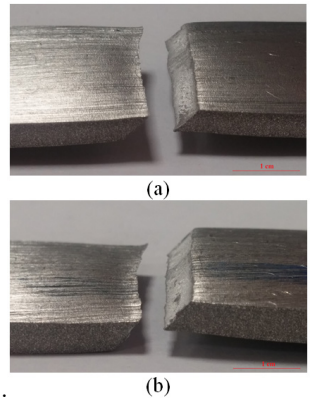

Fig. 6. Macro images of the fractured surfaces of the a) Alloy A, b) Alloy B

SEM images of fractured surfaces of the extruded alloys are shown in Figure 7. Although alloys have shear mode of fracture features macroscopically, their fracture surfaces are rather different at microscopic level. When the material is overloaded under uniaxial stress state, most of the structural alloys are damaged by a process consisting of microvoid nucleation, growth and coalescence. These microvoids nucleate in local strain discontinuities such as secondary phase particles, inclusions, grain boundaries and dislocations. As the stress concentration in the

material increase, the micro voids grow, coalesce and finally form a fracture surface. This type of fracture is known as ductile fracture. The Figure 7a demonstrates that the Alloy A was failed completely by ductile rupture which has large sized dimples caused by the coarse intermetallic particles and precipitates. However, fracture surface of Alloy B consists of small and shallow dimples. There are almost no dimples, but only quasi-brittle fracture zones along coarse brittle phase particles such as $Al_3(SiZr)$ (Figure 7b). This is closely related to the microstructural features after aging process. Furthermore, there are fine and relatively large dimples in the fracture surface of the Alloy B (Figure 7b) indicating non-uniform distribution and size of precipitate particles.

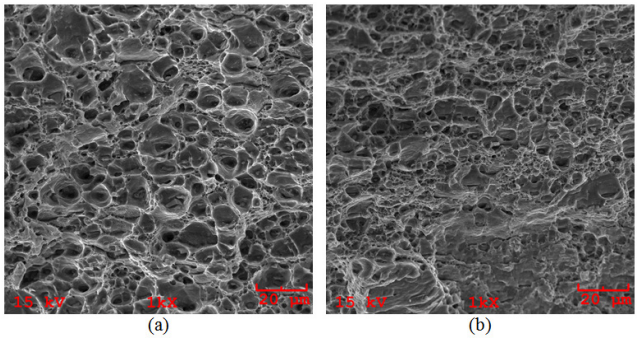

(a) (b)

Fig. 7. SEM images of the fractured surfaces of extruded alloys, a) Alloy A, b) Alloy B

Also, two structures of the Zr bearing precipitates mentioned above were detected by SEM examinations coupled with EDX spot analysis, on the fractured surface of Alloy B (Figure 8).

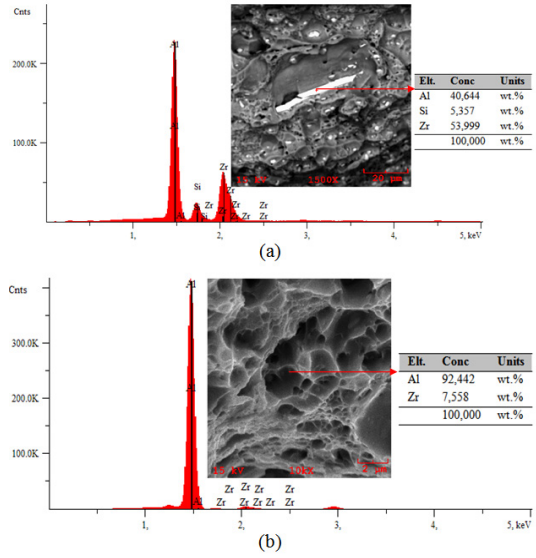

Fig. 8. SEM/EDX analyses of Zr bearing precipitates on fractured surface of Alloy B

4. Conclusions

The results show that artificial aging process has a significant influence on microstructural and mechanical properties because of the precipitation strengthening. Thus, the process parameters of precipitation strengthening such as aging time and temperature that give rise to the most favourable mechanical properties of Al-0.80Mg-0.85Si-0.3Zr alloys need to be determined. Following conclusions can be drawn from the present study in that respect:

1. Zr addition results in finer equiaxed dendritic microstructure of the alloys.
2. The ultimate tensile strength and the yield strength of the alloys with the Zr addition are improved by % 6.8 and % 19, respectively while elongation decreases from 18 % to 12 %.
3. Fractographic examinations of the fractured surfaces of the alloys reveal dimples indicating ductile fracture. With Zr addition, that is, with reduction in elongation and improvement of yield and ultimate strength, small and shallow dimples are apparent. Furthermore, with Zr addition although the elongation is small, fracture surface shows a mixed morphology with an increased number of dimples that are also small.

Acknowledgements

The authors gratefully acknowledge the financial support of the Scientific Research Projects Coordination Unit of Kocaeli University (Project number: 2013/072). The authors also thank Onat Profile and Alloy Industry and Trade Ltd. Co. for their assistance in providing the alloys used in the study and carrying out the tensile tests.

References

[1] Gowrishankar, M.C., Shravan, Rakesh, Rahul, Kını, A., Sharma, S.S. (2014). Effect of Artificial Aging on Strength and Wear Behaviour of Solutionized Aluminium 6061 Alloy. 3rd World Conference on Applied Sciences, Engineering & Technology. 27-29 September 2014 (pp. 388-393). Kathmandu, Nepal.

[2] Sharma, P., Khanduja, D. & Sharma, S. (2016). Dry sliding wear investigation of Al6082/Gr metal matrix composites by response surface methodology. *J Mater Res Technol*. (5)1, 29-36. DOI: 10.1016/j.jmrt.2015.05.001.

[3] Camero, S., Puchi, E.S. & Gonzalez, G. (2006). Effect of 0.1% vanadium addition on precipitation behaviour and mechanical properties of Al-6063 commercial alloy. *J Mater Sci*. 41, 7361-7373. DOI 10.1007/s10853-006-0794-0.

[4] Venkateswarlu, K., Pathak, L.C., Ray, A.K., Das, G., Verma, P.K., Kumar, M. & Ghosh, R.N. (2004). Microstructure, tensile strength and wear behaviour of Al-Sc alloy. *Materials Science and Engineering*: A, 383(2), 374-380. DOI: 10.1016/j.msea.2004.05.075.

[5] Jia, Z.H., Huang, H.L., Wang, X.L., Xing, Y. & Liu, Q. (2016). Hafnium in Aluminum Alloys: A Review. *Acta*

Metall. Sin. (Engl. Lett.) 29(2), 105-119. DOI 10.1007/s40195-016-0379-0.

[6] Meng, Y., Zhao, Z. & Cui, J. (2013). Effect of minor Zr and Sc on microstructures and mechanical properties of Al-Mg-Si-Cu-Cr-V alloys. *Trans. Nonferrous Met. Soc. China* 23, 1882-1889. DOI: 10.1016/S1003-6326(13)62673-4.

[7] Lityñska, L., Abou-ras, D., Kostorz, G. & Dutkiewicz, J. (2006). TEM and HREM study of Al_3Zr precipitates in an Al-Mg-Si-Zr alloy. *Journal of Microscopy*. 223, 182-184.

[8] Cerri, E. & Leo, P. (2005). Influence of severe plastic deformation on aging of Al-Mg-Si alloys. *Metal Science and Engineering A* 410-411, 226-229. DOI: 10.1016/j.msea.2005.08.135.

[9] Qingchun, X., Jing, Z., Haicheng, P., Lina, H. & Rongde, L. (2011). Effect of Scandium and Zirconium combination alloying on as-cast microstructure and mechanical properties of Al-4Cu-1.5Mg Alloy. *China Foundry*. 8(1), 137-140.

[10] Cabibbo, M. & Evangelista, E. (2006). A TEM Study of the Combined Effect of Severe Plastic Deformation and (Zr), (Sc+Zr)-Containing Dispersoids on an Al-Mg-Si Alloy. *J Mater Sci*. 41(16), 5329-5338. DOI: 10.1007/s10853-006-0306-2.

[11] Poková, M. & Cieslar, M. (2014). Study of twin-roll cast Aluminium alloys subjected to severe plastic deformation by equal channel angular pressing. IOP Conf. Ser.: Mater. Sci. Eng 63, conference 1.

[12] Mrówka-Nowotnik, G., Sieniawski, J. & Wierzbińska, M. (2007). Intermetallic phase particles in 6082 aluminum alloy. *Archives of Materials Science and Engineering.* 28(2), 69-76.

[13] Mrówka-Nowotnik, G. & Sieniawski, J. (2005). Influnce of heat treatment on the microstructure and mechanical properties of 6005 and 6082 aluminium alloys. *Journal of Materials Processing Technology*. 162-163, 367-372. DOI: 10.1016/j.jmatprotec.2005.02.115.

[14] Eivani, A.R., Zhou, J., Duszczyk, J. (2011). Microstructural Evolution During the Homogenization of Al-Zn-Mg Aluminum Alloys. Recent Trends in Processing and Degradation of Aluminium Alloys, Prof. Zaki Ahmad (Ed.) ISBN: 978-953-307-734-5, InTech, 477-516, DOI: 10.5772/34695.

[15] Edwards, G.A., Stiller, K., Dunlop, G.L. & Couper, M.J. (1998). The precipitation sequence in Al–Mg–Si alloys. *Acta Mater*. 46(11), 3893-904. DOI: 10.1016/S1359-6454(98)00059-7.

[16] Murayama, M., Hono, K., Miao, W. F. & Laughlin, D.E. (2001). The effect of Cu Additions on the precipitation kinetics in an Al–Mg–Si alloy with excess Si. *Metal Mater Trans* A 32(2), 239-246. DOI: 10.1007/s11661-001-0254-z.

[17] Demir, H. & Gündüz, S. (2009). The effects of aging on machinability of 6061 aluminium alloy. *Materials and Design*. 30(5), 1480–1483. DOI: 10.1016/j.matdes. 2008.08.007.

[18] Fang, X., Song, M., Li, K. & Du, Y. (2010). Precipitation sequence of An Aged Al-Mg-si Alloy. *J. Min. Metall. Sect. B-Metall*. 46(2)B, 171-180. DOI: 10.2298/JMMB1002171F.

[19] Fan, Y. (2012). Precipitation Strengthening of Aluminum by Transition Metal Aluminides. Master of Science Thesis, Worcester Polytechnic Institute, Worcester, MA.

[20] Liu, M., Wu, Z., Yang, R., Wei, J., Yu, Y., Skaret, P.C., Roven, H.J. (2015). DSC analyses of static and dynamic precipitation of an Al–Mg–Si–Cu aluminum alloy. Prog. Nat. Sci.: Materials International. 25, 153-158. DOI: 10.1016/j.pnsc.2015.02.004.

[21] Mukhopadhyay P. (2012). Alloy Designation, Processing, and Use of AA6xxx Series Aluminum Alloys. International Scholarly Research Network, ISRN Metallurgy. 1-15. http://dx.doi.org/10.5402/2012/165082.

[22] Røyset, J. & Ryum, N. (2005). Scandium in Aluminium Alloys. *Int. Mater. Rev*. 50(1), 19-44. DOI 10.1179/174328005X14311.

[23] Kahrıman, F. & Zeren, M. (2017). The effect of Zr on aging kinetics and properties of as-cast AA6082 alloy. *M. Inter Metalcast*. 11(2), 216-222. DOI: 10.1007/s40962-016-0047-1.